ADVANCED MATERIALS
www.advmat.de

Large-Area Atomic Layers of the Charge-Density-Wave Conductor $TiSe_2$

Hong Wang, Yu Chen, Martial Duchamp, Qingsheng Zeng, Xuewen Wang, Siu Hon Tsang, Hongling Li, Lin Jing, Ting Yu, Edwin Hang Tong Teo,* and Zheng Liu**

Layered transition metal (Ti, Ta, Nb, etc.) dichalcogenides are important prototypes for the study of the collective charge density wave (CDW). Reducing the system dimensionality is expected to lead to novel properties, as exemplified by the discovery of enhanced CDW order in ultrathin $TiSe_2$. However, the syntheses of monolayer and large-area 2D CDW conductors can currently only be achieved by molecular beam epitaxy under ultrahigh vacuum. This study reports the growth of monolayer crystals and up to 5×10^5 μm^2 large films of the typical 2D CDW conductor—$TiSe_2$—by ambient-pressure chemical vapor deposition. Atomic resolution scanning transmission electron microscopy indicates the as-grown samples are highly crystalline 1T-phase $TiSe_2$. Variable-temperature Raman spectroscopy shows a CDW phase transition temperature of 212.5 K in few layer $TiSe_2$, indicative of high crystal quality. This work not only allows the exploration of many-body state of $TiSe_2$ in 2D limit but also offers the possibility of utilizing large-area $TiSe_2$ in ultrathin electronic devices.

Layered transition metal dichalcogenides (TMDs) possess a whole spectrum of electronic properties covering insulators, semiconductors, semimetals, and metals.[1] Semiconducting TMDs members (MoS_2, WSe_2, etc.) have been widely investigated and show great potentials for high-performance electronic and optoelectronic devices, due to their high mobility and wide bandgap coverage.[2–4] The Ti-, Ta-, and Nb-based TMDs are another fascinating material category because of the coexistence and interplay of competing ordered phases including charge density wave (CDW) and superconductivity.[5–7] Among them, 1T-$TiSe_2$ provides an ideal opportunity to investigate the quantum phase transition between CDW and superconducting orders.[6,8,9] A CDW is a periodic modulation of both the electron density and the crystal lattice arising from an instability of the coupled electron–lattice system. In bulk $TiSe_2$, superconductivity emerges when CDW is suppressed by pressure or by intercalation of Cu atoms.[10,11] Reducing the system dimensionality is expected to lead to unprecedented and novel properties and phenomena. For instance, the CDW and superconducting order as well as their phase transitions could be tuned in 2D ultrathin $TiSe_2$ by an electric field.[8] On the other side, CDW can move and carry electric current when it is depinned by the application of a sufficient electric field.[12] 2D ultrathin CDW conductors with high transition temperatures ($TiSe_2$, TaS_2 and $TaSe_2$) are potentially suitable for applications in ultrafast memories,[13,14] oscillators[15] and logic circuits.[16,17]

A central issue in any thin-film application of $TiSe_2$ is the synthesis of large-area ultrathin films. $TiSe_2$ prepared by mechanically exfoliating bulk crystals are small flakes with uncontrolled thickness.[18–20] Currently, large-area $TiSe_2$ films can only be grown by molecular beam epitaxy (MBE) under ultrahigh vacuum (UHV).[21–24] The development of a facile growth routine of $TiSe_2$ is desirable. In the past few years, ambient-pressure chemical vapor deposition (CVD) has been developed for growing semiconducting TMDs thin layers such as MoS_2 and WSe_2.[25–31] However, the CVD synthesis of $TiSe_2$ has not been realized experimentally as conventional CVD routine is not applicable. Recently, Wang et al. reported the growth of small $TiSe_2$ flakes down to 4.5 nm by reaction of titanium and selenium in a sealed ampoule.[32] However, the synthesis of large-area $TiSe_2$ by CVD remains elusive. In addition, facile synthesis of monolayer $TiSe_2$ is another outstanding issue which limits the exploration of correlated phenomena such as CDW and superconductivity of $TiSe_2$ in 2D limit. For example, the spectroscopic signatures of CDW phase in monolayer $TiSe_2$

Dr. H. Wang, Prof. M. Duchamp, Dr. Q. Zeng, Dr. X. Wang, L. Jing, Prof. E. H. T. Teo, Prof. Z. Liu
School of Materials Science and Engineering
Nanyang Technological University
50 Nanyang Avenue, Singapore 639798, Singapore
E-mail: htteo@ntu.edu.sg; z.liu@ntu.edu.sg
Dr. H. Wang, Dr. H. Li, Prof. E. H. T. Teo
NOVITAS
Nanoelectronics Centre of Excellence
School of Electrical and Electronic Engineering
Nanyang Technological University
Singapore 639798, Singapore
Y. Chen, Prof. T. Yu
Division of Physics and Applied Physics
School of Physical and Mathematical Sciences
Nanyang Technological University
Singapore 637371, Singapore
E-mail: yuting@ntu.edu.sg
Dr. H. Wang, Prof. E. H. T. Teo
CNRS International NTU Thales Research Alliance (CINTRA)
50 Nanyang Drive, Singapore 637553, Singapore
Dr. S. H. Tsang
Temasek Laboratories@NTU
Nanyang Technological University
Singapore 637553, Singapore
The ORCID identification number(s) for the author(s) of this article can be found under https://doi.org/10.1002/adma.201704382.

DOI: 10.1002/adma.201704382

remain to be clarified.[20] Here, we demonstrate the synthesis of monolayer crystals and large-area films of $TiSe_2$ by salt-assisted ambient-pressure CVD. High-angle annular-dark-field scanning transmission electron microscopy (HAADF-STEM) characterization indicates that the as-grown films are highly crystalline 1T-$TiSe_2$. With low-temperature Raman spectroscopy technique, we investigated the spectroscopic signatures of CDW phase in CVD grown $TiSe_2$ with thickness down to 1.4 nm.

As described in the Experimental Section, we grew atomically thin $TiSe_2$ layers on SiO_2/Si substrates by salt-assisted CVD under atmospheric pressure. Partially oxidized Ti powder (TiO_x, $x \leq 2$) was first prepared and used as the Ti precursor for $TiSe_2$ growth. X-ray diffraction (XRD) analysis suggested the obtained power consisted mainly of Ti_2O, TiO, and Ti (Figure S1, Supporting Information). The TiO_x and LiCl powder mixture was loaded into the center of a tube furnace. Selenium powder was positioned at upstream and the heating temperature was ≈260 °C during the reaction. A mixture of argon and hydrogen was used as the carrier gas and provided reducing atmosphere to support the reaction. Previous studies suggested that a relatively low temperature near or below 600 °C should be used for synthesizing high-quality bulk $TiSe_2$ crystals.[8,33,34] For the melting salt-assisted CVD growth of ultrathin $TiSe_2$, LiCl was chosen because its melting point (≈605 °C) is very close to the suitable growth temperature (≈600 °C).

As shown by the optical image (**Figure 1**b), uniform ultrathin $TiSe_2$ crystals with triangular shape were deposited on a SiO_2/Si substrate. Atomic force microscope (AFM) height measurements (inset of Figure 1b) indicate the deposited $TiSe_2$ crystals have a typical thickness of ≈1.4 nm. Given the fact that ultrathin $TiSe_2$ is unstable under ambient conditions and the AFM was measured in air, small oxidized particles may form on the surface of $TiSe_2$, which makes the measured thickness slightly larger than that of air-stable TMDs such as MoS_2 and WS_2. Therefore, the measured thickness of 1.4 nm could be assigned to a monolayer.[19] $TiSe_2$ typically crystallizes in a layered 1T CdI_2-type structure (Figure 1a). Ti atoms form a hexagonal sheet and are sandwiched by two layers of hexagonally packed Se atoms. In our experiment, we find that $TiSe_2$ layers usually crystallize in triangular and hexagonal configurations on SiO_2/Si substrates (Figure 1c).

Raman spectroscopy was used to examine the lattice vibrational modes and to confirm the identity of the as-grown materials (Figure 1d; Figure S2, Supporting Information). According to previous theoretical and experimental studies,[33,35] there are two Raman-active modes in bulk 1T-$TiSe_2$, corresponding to A_{1g} and E_g symmetries with measured frequencies centered at 195–203 and around 134 cm^{-1}, respectively. The E_g mode corresponds to in-plane vibration of Se atoms, while the A_{1g} mode corresponds to out-of-plane vibration, as indicated in Figure 1e. Our Raman measurements were performed in vacuum to avoid the oxidation of samples in ambient conditions. The as-grown layers show two Raman peaks located at around 134 and 198 cm^{-1} (Figure 1d) which match very well with the E_g and A_{1g} optical phonon modes of 1T-$TiSe_2$. The weak peak around 300 cm^{-1} might be attributed to the overlap of the two phonon processes of $TiSe_2$ and the overtone of acoustic phonons of the silicon substrate.[33,34,36] Moreover, Raman intensity map of a few-layer triangular $TiSe_2$ (Figure S3, Supporting Information) indicates the Raman intensity is nearly uniform in each crystal. With the new developed synthesis technology, we were able to study the thickness dependence of Raman spectra of CVD grown $TiSe_2$ down to monolayer. As plotted in Figure 1f, the intensities of A_{1g} and E_g modes of few-layer (7.9 nm) $TiSe_2$ are higher than those of monolayer and thick (22 nm) $TiSe_2$, similar to the case of MoS_2, which is attributed to the optical interference effect between thin layers and SiO_2/Si substrates.[37]

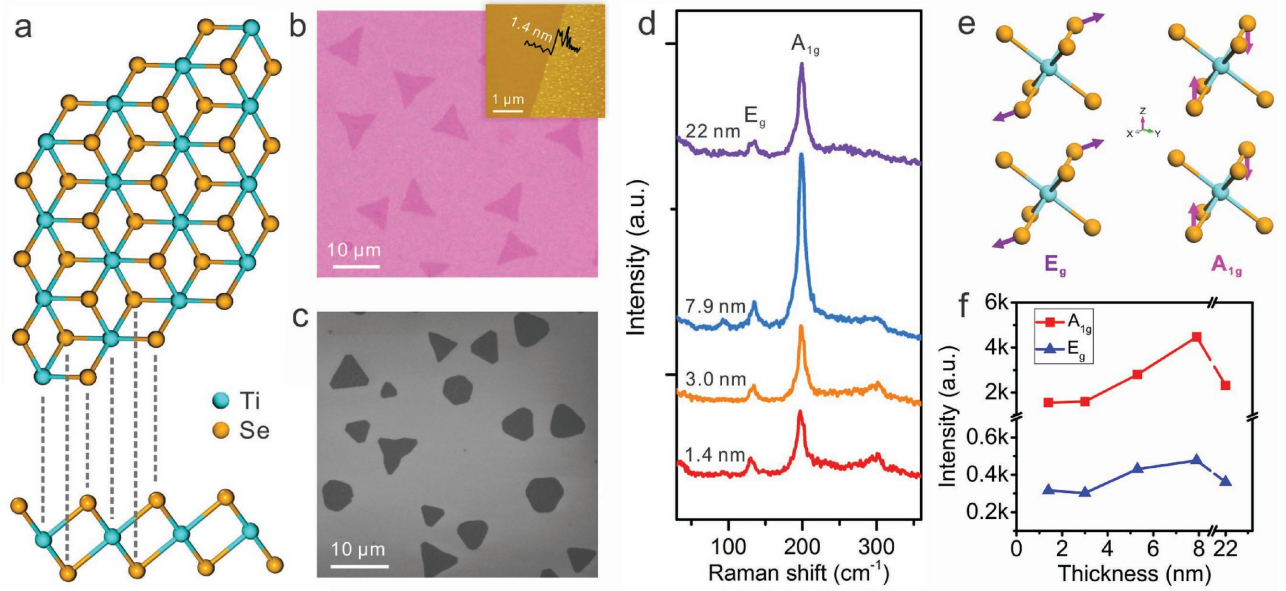

Figure 1. Atomic structure and characterization of atomic-thin $TiSe_2$ crystals. a) Top-down and side views of the atomic structure of 1T-$TiSe_2$. b) Optical image of monolayer $TiSe_2$ crystals grown on a SiO_2/Si substrate. AFM measurement (inset) indicates the thickness of $TiSe_2$ is ≈1.4 nm. c) SEM image showing the $TiSe_2$ crystals with different shapes. d) Raman spectra of the deposited $TiSe_2$ crystals with different thickness from 1.4 to 22 nm. e) Illustration of the E_g and A_{1g} crystal lattice vibrations in $TiSe_2$. f) The thickness dependence of Raman intensity of A_{1g} and E_g modes.

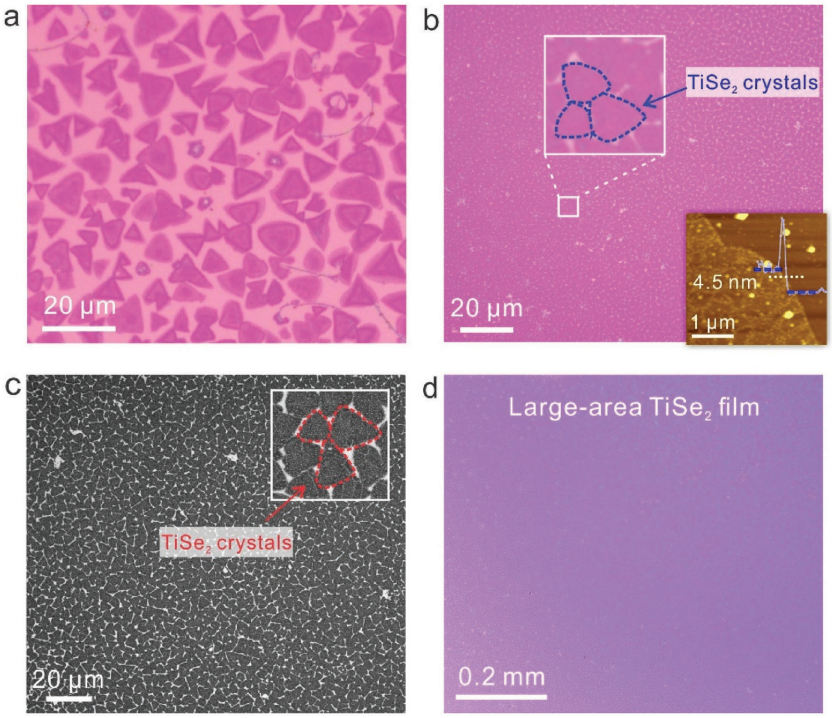

Figure 2. Large area atomically thin $TiSe_2$ films. a) High-density $TiSe_2$ nucleation with triangular shape. b) Optical and c) SEM images of the near-continuous $TiSe_2$ film. The inset of panel (b) and (c) indicates the film is made of approximately triangular $TiSe_2$ crystals. AFM height profile (lower inset in panel (b) suggests that the film is ≈4.5 nm thick. d) Optical image of a large-area $TiSe_2$ film covering approximately 5×10^5 μm^2.

In addition to individual $TiSe_2$ crystals, large-area $TiSe_2$ films can also be produced by adjusting the CVD parameters. By increasing the amount of precursors and the heating temperature of Se (see Methods in Supporting Information), high-density $TiSe_2$ few-layers (**Figure 2**a) and nearly continuous film (Figure 2b) were deposited on SiO_2/Si substrates. AFM height measurement (inset of Figure 2b) indicates the film is about 4.5 nm thick. Uniformly compact and approximately triangular crystals are observed by optical and scanning electron microscopy (SEM) (inset of Figure 2b,c), which suggests that the large film is made of high crystalline $TiSe_2$ crystals. Figure 2d shows a ≈5×10^5 μm^2 large-area $TiSe_2$ film grown on a SiO_2/Si substrate. Meanwhile, it was noted that no nucleation of $TiSe_2$ on substrates could be observed without the addition of LiCl salt (Figure S4, Supporting Information). The reason is that titanium oxide alone is not a suitable CVD precursor due to its very high melting point (>1500 °C). Previous studies indicate that salts (LiCl, NaCl, $CaCl_2$, etc.) react with molybdenum/tungsten oxides to give volatile oxychlorides.[38–40] Therefore, it is suggested that titanium oxychlorides may form as intermediates in our CVD reaction, and further react with selenium to produce $TiSe_2$. Due to the highly volatile property of titanium oxychlorides, the vapor pressure of titanium precursor is greatly enhanced, therefore making the synthesis of large-area $TiSe_2$ films on substrates possible.

The crystallographic structure and the chemical composition of the ultrathin $TiSe_2$ layers were further characterized by atomic resolution HAADF-STEM imaging and energy-dispersive X-ray spectrometry (EDX). The as-grown few-layer $TiSe_2$ on SiO_2/Si substrate was coated with a thin layer of polymethyl-methacrylate (PMMA), and then transferred onto a TEM grid by etching SiO_2 in hydrofluoric acid (HF). **Figure 3**a shows a lower magnification STEM image of the $TiSe_2$ film. Figure 3b shows an atomically resolved HAADF-STEM image of the dark area (as indicated by the yellow circle in Figure 3a). HAADF-STEM is sensitive to average atomic number of the elements, a bright contrast is associated to an element with a larger atomic number. The overall empty hexagonal structure is formed by the Se (Z = 34) atoms. The lighter Ti (Z = 22) atoms are just seen in the middle of the hexagon (shown by arrows in Figure 3c). The STEM image can be perfectly overlaid with the 1T-$TiSe_2$ atomic model (Figure 3c), which confirms the 1T structure of the as-grown material. In addition, EDX-STEM mapping (Figure 3d,e) and spectrum (Figure 3f) of the area indicated by the red square frame in Figure 3a confirms the thin film is composed of Se and Ti atoms. The EDX maps show an excess of Se atoms which aggregate on the surface of the film, forming some rod-like structures, while Ti atoms are evenly distributed in the layer.

Understanding the dependence of CDW transition properties on film thickness is essential for any thin-film application. Therefore, we use low-temperature Raman spectroscopy to investigate the CDW transition in the as-grown $TiSe_2$. To avoid oxidation, the $TiSe_2$ samples were sealed within a chamber in an Ar glove box immediately after CVD growth and then transferred for Raman test under vacuum. The total sample exposure time in air is less than 1 min. The variable-temperature Raman spectra of $TiSe_2$ with the thicknesses of 22, 3.7, and 1.4 nm are displayed in the bottom panels in **Figure 4**. For ease of comparison, the results are further plotted as contour maps of Raman intensity versus temperature and frequency (top panels in Figure 4). For $TiSe_2$ samples at 80 K, in addition to the original A_{1g} and E_g peaks, two new modes including a clear and strong peak near 110 cm^{-1} and a broad one near 75 cm^{-1} emerge in the Raman spectrum (Figure 4a,b). According to the previous studies of bulk $TiSe_2$, these two modes were attributed to CDW amplitude modes (A_{1g}-CDW and E_g-CDW) which resulted from the folding of transverse acoustic phonons from the L point at the Brillouin zone surface to zone center due to CDW superlattice formation.[33,35] Notably, for the monolayer (1.4 nm thick) $TiSe_2$, the A_{1g}-CDW Raman mode is still clearly visible, although slightly broader compared to thicker samples (Figure 4e,f). When temperature increases to higher than 80 K, the broad E_g-CDW peak at 75 cm^{-1} becomes too broad to be discernible, while the A_{1g}-CDW mode remains detectable. Therefore, we use the A_{1g}-CDW mode as an indicator for the presence of CDW in CVD-grown $TiSe_2$.

The integrated intensities of the A_{1g}-CDW mode are displayed as a function of temperature in **Figure 5**a. One can see

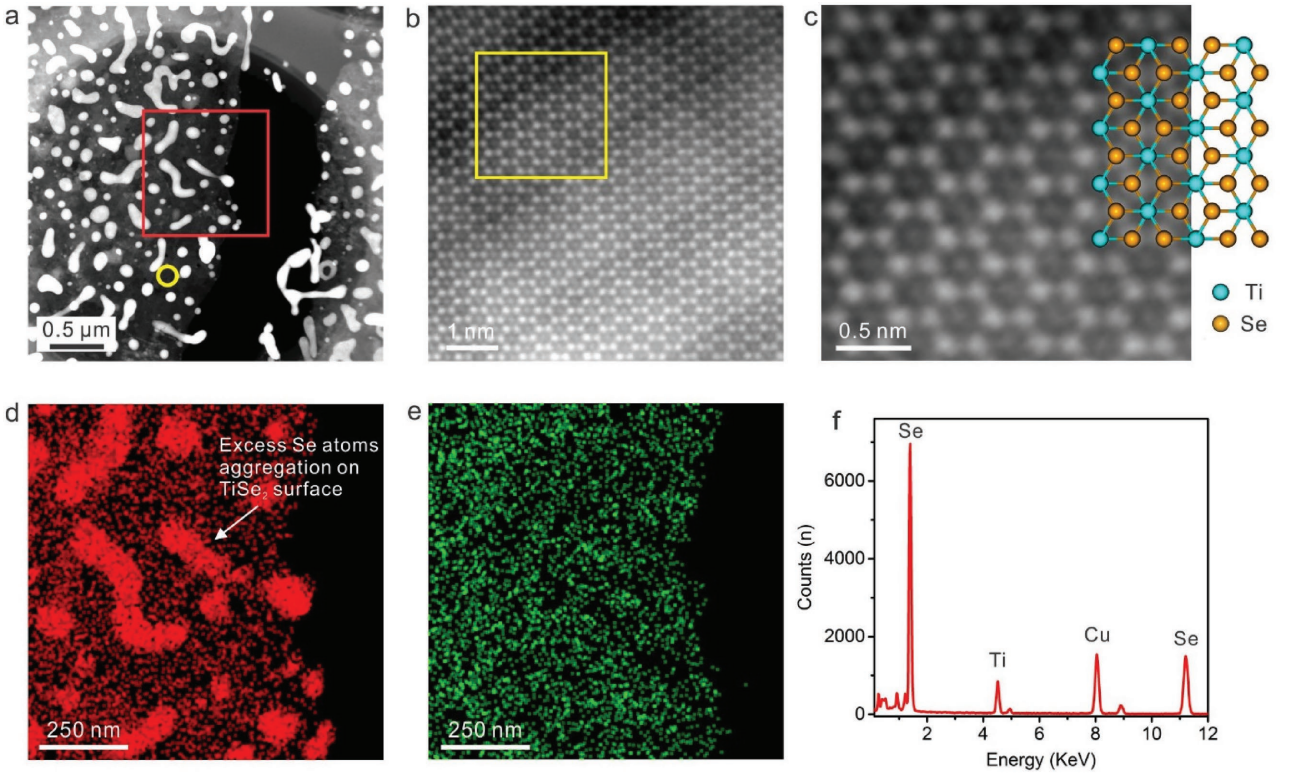

Figure 3. HAADF-STEM and EDX characterizations of the as-grown $TiSe_2$ layers. a) A low magnification HAADF-STEM image showing a large region of $TiSe_2$. b,c) Atomic-resolution HAADF-STEM images and the associated structural model of the 1T-$TiSe_2$. d) Se and e) Ti elemental EDX map and f) averaged EDX spectrum of the region shown in (a). The Cu signal in the EDX spectra comes from the Cu TEM grid.

that for a given sample, the intensity of CDW mode decreases with increasing temperature, and finally drops to zero, indicating the transition from CDW to normal phase. The CDW onset temperature is around 187.5 K for 22 nm thick $TiSe_2$, and increases to around 212.5 K for a 3.7 nm thick sample. The thickness–temperature phase diagram for CVD-grown $TiSe_2$ is summarized in Figure 5b. It is noted that the CDW order is enhanced in few-layer $TiSe_2$ as compared with a much thicker (22 nm) sample. The slightly lower onset temperature (around 202.5 K, Figure S5, Supporting Information) in 1.4 nm thick sample might result from the higher instability of monolayer $TiSe_2$ compared with few-layers. The short air exposure before Raman measurement as well as the weak laser irradiation during the measurement could induce disorders and suppress the CDW order in monolayer $TiSe_2$.[33] To our knowledge, this is the first Raman spectroscopic observation of CDW phase transition in monolayer $TiSe_2$.

The as-grown few-layer $TiSe_2$ shows a transition temperature (≈212.5 K) close to the reported value of MBE-grown 3–6 layer samples (≈205 K) revealed by angle-resolved photoemission spectroscopy (ARPES) and XRD.[23,24] Therefore, the crystalline quality of few-layer CVD-$TiSe_2$ is comparable with that prepared by MBE. Additionally, ARPES and XRD experiments suggest an enhanced transition temperature (≈232 K) in MBE-grown monolayer $TiSe_2$, which is significantly higher than that of CVD monolayer $TiSe_2$ (≈202.5 K) deduced from Raman spectroscopy. The main reason is probably that ARPES and XRD experiments were measured in situ after MBE growth under UHV, while Raman test was conducted ex situ after CVD growth in non-UHV environment. As discussed earlier, disorders might be easily induced in CVD monolayer $TiSe_2$ before and during Raman measurement, resulting in a lower CDW transition temperature.

In conclusion, we demonstrated the synthesis of mono- and few-layer $TiSe_2$ crystals and large-area (≈5×10^5 μm^2) films on insulating SiO_2/Si substrates. HAADF-STEM imaging confirms the as-grown samples are highly crystalline 1T-phase $TiSe_2$. Low-temperature Raman measurement reveals the thickness-dependent CDW phase transition in the as-grown samples. The transition temperature of 212.5 K in few layers suggests the CVD $TiSe_2$ films crystallize in high-quality. Our work has implications for the synthesis and development of other fascinating 2D charge ordering and superconducting materials (TaS_2, $NbSe_2$, $TaSe_2$, etc).

Experimental Section

CVD Growth of Mono- and Few-Layer $TiSe_2$ Crystals: Titanium oxide (TiO_x) precursor was prepared by heating titanium powder (Alfa Aesa, 325 mesh, 99.5%) at a temperature of ≈820 °C for 15 min in air. The bottom dark grey powder was used as the TiO_x precursor. The synthesis of $TiSe_2$ was conducted in a 1 in. OD fused quartz tube heated by a Lindberg/Blue M (TF55035C-1) split-hinge furnace. The TiO_x (60 mg) and LiCl (2.5 mg, Sigma-Aldrich, 99.99%) precursors were mixed in an alumina boat and then positioned in the center of the furnace. 285 nm SiO_2/Si substrate was placed just above the powder mixture with the polished side face down. Selenium powder was placed at the

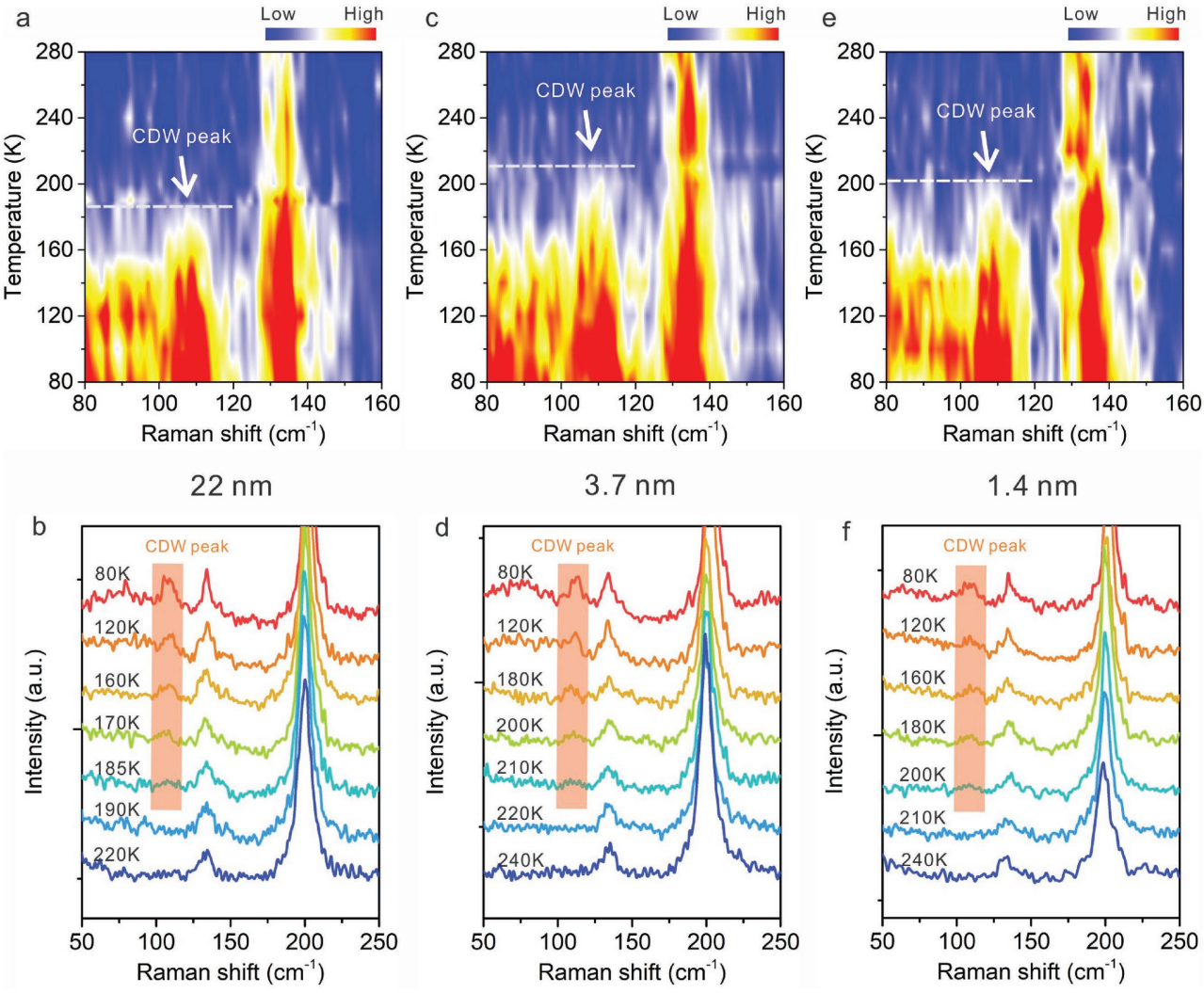

Figure 4. Raman spectra showing the CDW transition in the as-grown $TiSe_2$ for different thickness. a,c,d) Raman intensity maps as a function of Raman shift (horizontal axis) and temperature (vertical axis) for a) 22 nm, c) 3.7 nm, and e) 1.4 nm thick $TiSe_2$ crystals. b,d,f) Representative Raman spectra of b) 22 nm, d) 3.7 nm, and f) 1.4 nm thick $TiSe_2$ samples at selected temperatures.

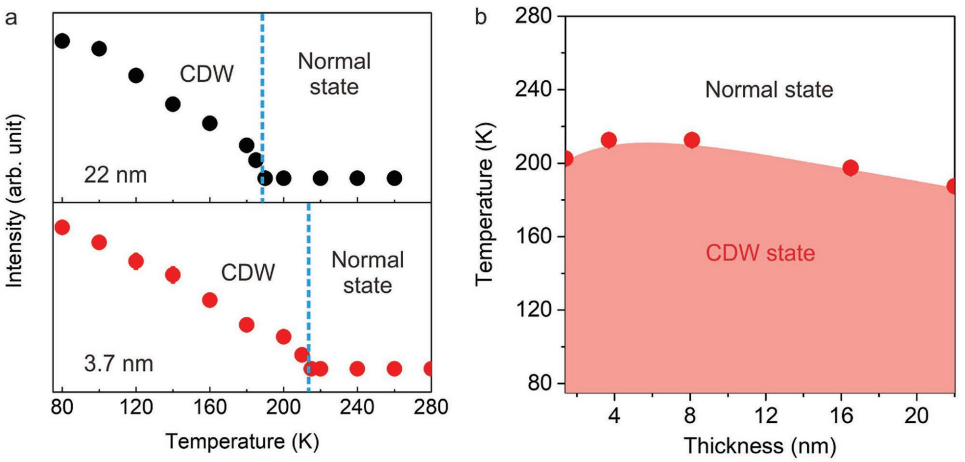

Figure 5. a) Temperature-dependent scattering intensities of the A_{1g}-CDW mode showing that the mode vanishes around 187.5 and 212.5 K for 22 and 3.7 nm thick $TiSe_2$, respectively. b) Thickness–temperature phase diagram for $TiSe_2$ grown by CVD.

upstream of the quartz tube where the temperature is ≈260 °C during the reaction. 80 sccm (cubic centimeters per minute) Ar and 15 sccm H_2 were used as carrier gases. The furnace was heated to 600 °C in 14 min and maintained at this temperature for 13 min to allow the synthesis of $TiSe_2$ layers. After growth, hydrogen was turned off and the furnace was rapidly cooled to room temperature under 180 sccm Ar. The above growth condition allows the deposition of high-density monolayer $TiSe_2$ crystals, plus a small proportion of few-layer and even thicker $TiSe_2$ layers on the nearby SiO_2/Si substrates. All the Raman spectra in this work were collected on $TiSe_2$ layers grown under the same CVD condition as described above.

CVD Growth of Large-Area Few-Layer $TiSe_2$ Films: Large-area $TiSe_2$ films were synthesized by increasing the amount of the precursors (TiO_x: 80 mg, LiCl: 3.5 mg) and setting the heating temperature of selenium at ≈300 °C during growth period, while keeping all other growth parameters identical).

Preparation of STEM Sample: A thin PMMA film was spin-coated on top of $TiSe_2$ layers grown on 285 nm SiO_2/Si and cured at 130 °C for 6 min in an Ar glove box. The PMMA/$TiSe_2$ film was detached from the substrate by etching SiO_2 layer in HF. After rinsed in DI water, it was scooped up by a TEM grid and dried in an Ar glove box. Finally, PMMA was removed by acetone.

Characterizations: AFM images were taken using the Asylum Research Cypher AFM in tapping mode. HAADF-STEM images were recorded using a probe corrected Jeol ARM200F using an inner collection semi-angle of 68 mrad and a convergence semi-angle of 30 mrad at 80 keV. Raman measurements were conducted in vacuum by a Witec system with 50× objective lens and a 2400 lines mm^{-1} grating under 532 nm laser excitation. The laser power is kept below 0.6 mW. For low temperature Raman measurements, a temperature-controlled evacuated chamber cooled by liquid nitrogen is used for preventing the potential oxidation and local heating of the $TiSe_2$ samples under laser irradiation.

Supporting Information

Supporting Information is available from the Wiley Online Library or from the author.

Acknowledgements

H.W., Y.C., and M.D. contributed equally to this work. This work was supported by the Singapore National Research Foundation under NRF RF Award No. NRF-RF2013-08, the start-up funding from Nanyang Technological University (Grant Nos. M4081137.070 and M4081924.070), Tier 2 MOE2016-T2-2-153, MOE2016-T2-1-131 (S), MOE2015-T2-2-007, Tier 1 RG164/15. Y.C. and T.Y. thank the support of Ministry of Education AcRF Tier 1 RG100/15. The electron microscopy imaging was performed at the Facility for Analysis, Characterization, Testing and Simulation (FACTS) in Nanyang Technological University, Singapore.

Conflict of Interest

The authors declare no conflict of interest.

Keywords

2D materials, charge density waves, transition metal dichalcogenides

Received: August 3, 2017
Revised: November 20, 2017
Published online: January 10, 2018

[1] P. Miró, M. Audiffred, T. Heine, *Chem. Soc. Rev.* **2014**, *43*, 6537.
[2] Q. H. Wang, K. Kalantar-Zadeh, A. Kis, J. N. Coleman, M. S. Strano, *Nat. Nano* **2012**, *7*, 699.
[3] M. Buscema, J. O. Island, D. J. Groenendijk, S. I. Blanter, G. A. Steele, H. S. J. van der Zant, A. Castellanos-Gomez, *Chem. Soc. Rev.* **2015**, *44*, 3691.
[4] D. Jariwala, V. K. Sangwan, L. J. Lauhon, T. J. Marks, M. C. Hersam, *ACS Nano* **2014**, *8*, 1102.
[5] X. Xi, L. Zhao, Z. Wang, H. Berger, L. Forró, J. Shan, K. F. Mak, *Nat. Nano* **2015**, *10*, 765.
[6] Y. I. Joe, X. M. Chen, P. Ghaemi, K. D. Finkelstein, G. A. de la Pena, Y. Gan, J. C. T. Lee, S. Yuan, J. Geck, G. J. MacDougall, T. C. Chiang, S. L. Cooper, E. Fradkin, P. Abbamonte, *Nat. Phys.* **2014**, *10*, 421.
[7] M. Calandra, *Nat. Nano* **2015**, *10*, 737.
[8] L. J. Li, E. C. T. O'Farrell, K. P. Loh, G. Eda, B. Özyilmaz, A. H. Castro Neto, *Nature* **2016**, *529*, 185.
[9] M. Calandra, F. Mauri, *Phys. Rev. Lett.* **2011**, *106*, 196406.
[10] A. F. Kusmartseva, B. Sipos, H. Berger, L. Forro, E. Tutiš, *Phys. Rev. Lett.* **2009**, *103*, 236401.
[11] E. Morosan, H. Zandbergen, B. Dennis, J. Bos, Y. Onose, T. Klimczuk, A. Ramirez, N. Ong, R. Cava, *Nat. Phys.* **2006**, *2*, 544.
[12] T. Adelman, S. Zaitsev-Zotov, R. Thorne, *Phys. Rev. Lett.* **1995**, *74*, 5264.
[13] I. Vaskivskyi, I. A. Mihailovic, S. Brazovskii, J. Gospodaric, T. Mertelj, D. Svetin, P. Sutar, D. Mihailovic, *Nat. Commun.* **2016**, *7*, 11442.
[14] D. Mihailovic, D. Dvorsek, V. Kabanov, J. Demsar, L. Forro, H. Berger, *Appl. Phys. Lett.* **2002**, *80*, 871.
[15] G. Liu, B. Debnath, T. R. Pope, T. T. Salguero, R. K. Lake, A. A. Balandin, *Nat. Nano* **2016**, *11*, 845.
[16] J. Renteria, R. Samnakay, C. Jiang, T. R. Pope, P. Goli, Z. Yan, D. Wickramaratne, T. T. Salguero, A. G. Khitun, R. K. Lake, A. A. Balandin, *J. Appl. Phys.* **2014**, *115*, 034305.
[17] R. Samnakay, D. Wickramaratne, T. R. Pope, R. K. Lake, T. T. Salguero, A. A. Balandin, *Nano Lett.* **2015**, *15*, 2965.
[18] L. J. Li, W. J. Zhao, B. Liu, T. H. Ren, G. Eda, K. P. Loh, *Appl. Phys. Lett.* **2016**, *109*, 141902.
[19] D. L. Duong, G. Ryu, A. Hoyer, C. Lin, M. Burghard, K. Kern, *ACS Nano* **2017**, *11*, 1034.
[20] P. Goli, J. Khan, D. Wickramaratne, R. K. Lake, A. A. Balandin, *Nano Lett.* **2012**, *12*, 5941.
[21] P. Chen, Y. H. Chan, X. Y. Fang, Y. Zhang, M. Y. Chou, S. K. Mo, Z. Hussain, A. V. Fedorov, T. C. Chiang, *Nat. Commun.* **2015**, *6*, 8943.
[22] K. Sugawara, Y. Nakata, R. Shimizu, P. Han, T. Hitosugi, T. Sato, T. Takahashi, *ACS Nano* **2016**, *10*, 1341.
[23] P. Chen, Y. H. Chan, M. H. Wong, X. Y. Fang, M. Y. Chou, S. K. Mo, Z. Hussain, A. V. Fedorov, T. C. Chiang, *Nano Lett.* **2016**, *16*, 6331.
[24] X.-Y. Fang, H. Hong, P. Chen, T.-C. Chiang, *Phys. Rev. B* **2017**, *95*, 201409.
[25] J.-K. Huang, J. Pu, C.-L. Hsu, M.-H. Chiu, Z.-Y. Juang, Y.-H. Chang, W.-H. Chang, Y. Iwasa, T. Takenobu, L.-J. Li, *ACS Nano* **2013**, *8*, 923.
[26] J. H. Ahn, M. J. Lee, H. Heo, J. H. Sung, K. Kim, H. Hwang, M. H. Jo, *Nano Lett.* **2015**, *15*, 3703.
[27] M. Hafeez, L. Gan, H. Li, Y. Ma, T. Zhai, *Adv. Mater.* **2016**, *28*, 8296.
[28] X. Duan, C. Wang, J. C. Shaw, R. Cheng, Y. Chen, H. Li, X. Wu, Y. Tang, Q. Zhang, A. Pan, J. Jiang, R. Yu, Y. Huang, X. Duan, *Nat. Nano* **2014**, *9*, 1024.
[29] Y. Zhou, Y. Nie, Y. Liu, K. Yan, J. Hong, C. Jin, Y. Zhou, J. Yin, Z. Liu, H. Peng, *ACS Nano* **2014**, *8*, 1485.
[30] Y. Kim, B. Kang, Y. Choi, J. H. Cho, C. Lee, *2D Mater.* **2017**, *4*, 025057.
[31] C. Cong, J. Shang, X. Wu, B. Cao, N. Peimyoo, C. Qiu, L. Sun, T. Yu, *Adv. Opt. Mater.* **2013**, *2*, 131.
[32] J. Wang, H. Zheng, G. Xu, L. Sun, D. Hu, Z. Lu, L. Liu, J. Zheng, C. Tao, L. Jiao, *J. Am. Chem. Soc.* **2016**, *138*, 16216.

[33] J. Holy, K. Woo, M. Klein, F. Brown, *Phys. Rev. B* **1977**, *16*, 3628.
[34] S. Uchida, S. Sugai, *Physica B+C* **1981**, *105*, 393.
[35] C. Snow, J. Karpus, S. Cooper, T. Kidd, T.-C. Chiang, *Phys. Rev. Lett.* **2003**, *91*, 136402.
[36] P. A. Temple, C. Hathaway, *Phys. Rev. B* **1973**, *7*, 3685.
[37] S.-L. Li, H. Miyazaki, H. Song, H. Kuramochi, S. Nakaharai, K. Tsukagoshi, *ACS Nano* **2012**, *6*, 7381.
[38] S. Li, S. Wang, D.-M. Tang, W. Zhao, H. Xu, L. Chu, Y. Bando, D. Golberg, G. Eda, *Appl. Mater. Today* **2015**, *1*, 60.
[39] K. V. Manukyan, K. G. Kirakosyan, Y. G. Grigoryan, O. M. Niazyan, A. V. Yeghishyan, A. G. Kirakosyan, S. L. Kharatyan, *Ind. Eng. Chem. Res.* **2011**, *50*, 10982.
[40] M. Erdoğan, İ. Karakaya, *Metallurg. Mater. Trans. B* **2010**, *41*, 798.